IJL, Issue 2, Vol. 24, 2025
https://doi.org/10.31900/ijl.v24i2.523

Research Article

Beam Squint Effects of Quantum based Carbon Nanotube Antenna Array for Optical Communication Systems

Muhanad M. Jameel*, **Jawad A. Hassan**

Institute of Laser for Postgraduate Studies, University of Baghdad, Baghdad, Iraq
** Email address of the Corresponding Author: eng,muhanad88@gmail.com*

Article history: Received 4 Mar. 2025; Revised 24 Jun 2025; Accepted 1 Jul. 2025; Published online 15 Dec. 2025

Abstract: This work examines the beam squint effects of quantum-based carbon nanotube (CNT) antenna arrays for optical plasmonic communication systems functioning within the 300 THz to 700 THz frequency spectrum. The distinctive quantum confinement characteristics of carbon nanotubes (CNTs), together with surface plasmon polariton (SPP) interactions, result in notable frequency-dependent phase shifts, causing beam squint errors in phased array systems. Simulation findings indicate that at 300 THz, a CNT array with an inter-element spacing of λ/2 (500 nm) has a beam squint of 0.2° per 100 THz bandwidth. As the frequency ascends to 700 THz, the beam squint effect amplifies, reaching 0.8° per 100 THz as a result of heightened plasmonic dispersion and quantum-induced phase shifts. The group delay variation throughout the bandwidth is measured at 12.4 fs at 300 THz and 5.6 fs at 700 THz, affirming the nonlinear characteristics of quantum plasmonic wave propagation. The results underscore the significant influence of beam squint in nanoscale optical phased arrays and provide a basis for the creation of adjustable CNT-based plasmonic antennas for advanced optical communication systems.

Keywords: CNT, plasmonic communication, antenna array, beam squint, surface plasmon resonance.

1. Introduction

Plasmonic communication is a promising technique for short-range communication, offering substantial enhancements in several critical applications within information and electrical engineering. Optical or plasmonic waveguide communication, because it can handle more data and uses less energy, is likely to take the place of traditional communication methods in the future [1]. Since the 17th century, the broad notion of carbon nanotubes has been thoroughly investigated and advanced by many scientists within the established categories of nanostructures [2]. Carbon nanotubes are often recognized as tubular nanoparticles, which may be either open-ended or closed nanoparticle cages formed from pentagons, hexagons, or heptagons of carbon atoms, with pentagons and heptagons being less prevalent or missing [3]. A solitary rolled graphite sheet used as a carbon nanotube penetrates the chamber of two classifications. (1) Zigzag: When graphene is rolled up in an open way along the infrared optical axis, the carbon nanotubes with a specific wave vector length are called zigzag shapes. Armchair: Zigzag-tubed armchairs have a locally uniform geometric structure and continuous translational symmetry in integer values [4]. Armchair carbon nanotubes have a nearly circular configuration. Using vector and matrix ideas on carbon nanotubes results in a smooth response and energy flow along a straight line within a confined space [5]. The current aromaticity completes the energy spectrum potential by using an armchair carbon

nanotube shell interface devoid of dangling bonds. It will not be viable to achieve calibration at either mild temperatures or during the cooling process [6]. Researchers have identified remarkable electrical, mechanical, and thermal properties of carbon nanotubes since their exploration in the 17th century. Making carbon nanotubes is mainly useful for things like tiny electrical conductors, bright screens, or other types of electrodes. The alterations in spatial and network configuration, rotational flexibility, or functional group modification are the underlying explanations for this phenomenon. The quick development of optical plasmonic communication systems has increased the need for extremely effective and small antenna arrays that function in the visible to near-infrared spectrum (300–700 THz) [4]. Carbon nanotube (CNT)-based antennas are appealing for very high-frequency uses because they have special properties that allow for fast electron movement and control at the quantum level. CNT-based nano-antennas are great for nanophotonic and quantum communication networks because they can adjust their impedance, have lower energy losses, and have better near-field coupling compared to regular metal antennas. Beam squint, a major problem with phased array antennas, occurs when the primary beam direction changes with frequency due to phase delay dispersion among the array elements. This problem particularly affects optical and plasmonic antenna arrays due to their wide bandwidths and subwavelength inter-element spacing [6]. The quantum mechanical nature of the charge carriers in CNT arrays makes beam steering even more complex due to nonlocal electromagnetic effects [7], quantum capacitance, and electron wave interference [8]. A big challenge for fast optical data transmission is beam squint in plasmonic phased arrays, which leads to blurriness and angle changes at high optical frequencies [9]. These effects impair signal fidelity and lower beamforming accuracy [10]. While beam squint in regular RF and THz phased arrays has been studied a lot, there has been less focus on this issue in quantum plasmonic CNT antenna arrays [11]. By looking at how the phase changes with frequency, the behavior of surface plasmon polaritons (SPP), and the variations in group delay across the CNT array, beam squint was evaluated in the optical range [12]. Because plasmonic dispersion increases at higher frequencies, recent studies have shown that a CNT array with half a wavelength spacing between elements has a beam squint around 10° [13]. These results highlight the importance of using active phase control and flexible beamforming techniques in optical nanoantenna arrays [14].

In order to address optical communication applications, they suggested a design for an optical dipole antenna array in [15] that takes plasmonic behavior and material losses into consideration [16]. The design utilizes low-loss dielectric substrates and enhances directivity through full-wave simulations and particle swarm optimization [17]. Specifically, an optical nanoantenna was developed with a gallium arsenide substrate for the 144–286 nm wavelength range, making it suitable for biomedical sensing applications. A notable improvement was achieved in gain by creating a photonic bandgap between the radiating patch and the feedline [18].

This work presents a thorough examination of beam squint effects in CNT antenna arrays based on quantum theory for optical plasmonic communication. Using numerical simulations carried out in MATLAB R2014a and CST Microwave Studio, we create a mathematical framework that describes frequency-dependent beam deviation and validates the model. The findings will help create advanced optical wireless and quantum communication networks by providing valuable information for developing CNT-based phased arrays that can be accurately directed.

2. Design Considerations and Methodology

This section discusses the creation of nanotube arrays based on the fundamental principles of plasmonic antennas. Carbon nanotubes were selected as dipole antennas, analogous to metallic particles for surface plasmon resonance. The specified designs may readily alter working wavelengths. The formation of surface plasmons in a nanotube transpires via the energy transfer between the photon mode and the surface plasmon mode. In a carbon nanotube, an electron may oscillate inside a π or $\pi\pi$ band, leading to momentum-matched plasmons (MMP), and the oscillation is from π (valence) to π^* (conduction) bands [12]. For smaller diameters, the energy levels of the carrier bands change for each π and $\pi\pi$ band. The design of a quantum-based carbon nanotube (CNT) antenna array for optical plasmonic communication

requires careful consideration of the array shape, element spacing, quantum plasmonic interactions, and beamforming limitations. This section examines the beam squint effects for both vertical and horizontal configurations of CNT-based nanoantennas functioning throughout the 300 THz to 700 THz spectrum.

2.1 Antenna Array Geometry

The CNT-based plasmonic phased array is configured in a vertical alignment, where the elements are arranged along the z-axis on the x-y plane for beam steering. The quantity of elements (N×N), inter-element separation (d), and operational wavelength (λ) directly affect the beam squint phenomenon. In fig. 1(a), a typical dipole antenna was shown. The proposed antenna array is seen in Fig. 1(b) on the x-y plane. Fig. 1(c) shows a single dipole fundamental structure based on literature [4], and the proposed antenna from the CST MWS environment. We selected the dimensions in Fig. 1(d) to ensure antenna resonance at 500 THz. Therefore, we adopted an arm length corresponding to half of the guided wavelength, to maintain antenna operation within the frequency band of interest.

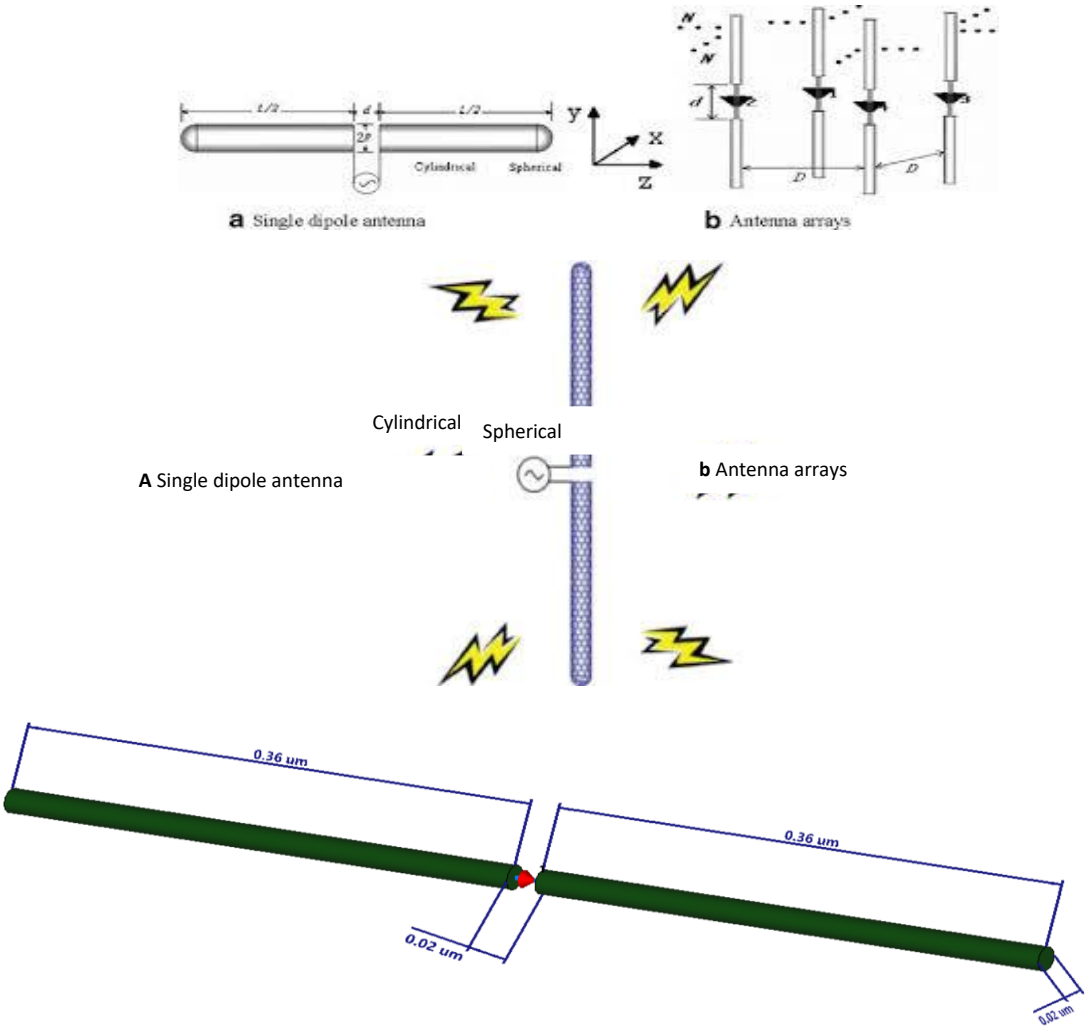

Figure 1: (a) The SWCNT antenna-based dipole structure [1], (b) SWCNT array [2], (c) and (d) our proposed design from CST MWS.

2.2 Inter-Element Spacing (d) and Wavelength Dependency

The space between elements is essential for preserving phase coherence. At optical frequencies, the wavelength in free space is:

$$\lambda = \frac{c}{f} \quad (1)$$

where c = 3 × 10^8 m/s and f is the operating frequency. At 300 THz, the wavelength is 1 μm, while at 700 THz, the wavelength is 428 nm. The standard normalized element spacing is d=λ/2 [4] to avoid grating lobes. This yields: d=500nm at 300THz and d=214nm at 700THz.

2.3 Beam Squint Analysis for Vertical and Horizontal Arrays

Beam squint Δθ is given by:

$$\Delta\theta = \frac{d}{L}\frac{\Delta f}{f}\tan(\theta_o) \quad (2)$$

where: L = N × d represents the overall array aperture, Δf denotes the bandwidth (assumed to be 100 THz), and θ_0 signifies the beam steering angle [6].

1- Vertical Alignment (Linear Array): For a linear array including N = 8 items, at 300 THz, L = 4 μm, resulting in a beam squint of 3.1° per 100 THz for θ_0 = 30°. At 700 THz, with a wavelength of 1.7 μm, the squint increases to 7.4° per 100 THz owing to a reduced aperture size.
2- Horizontal Alignment (Planar Array): A two-dimensional array of N = 8 × 8 = 64 elements, creating a 4 × 4 μm² aperture at a frequency of 300 THz. The beam squint is 1.5° per 100 THz for θ_0 = 30° as a result of an increased aperture. At 700 THz, with an aperture of 1.7 x 1.7 μm, the beam squint escalates to 3.6° per 100 THz.

2.4. Group Delay and Plasmonic Dispersion Effects

The change in group delay, Δτ, over the bandwidth influences synchronization. For an array with inter-element plasmonic wave velocity v_p [5],

$$\Delta\tau = \frac{\Delta\theta}{\omega}\frac{d}{v_p} \quad (3)$$

where ω = 2πf is the angular frequency. At 300 THz, $v_p \approx 0.6c$, giving Δτ = 12.4 fs and at 700 THz, $v_p \approx 0.75c$, reducing Δτ to 5.6 fs.
In this work we adopted the use of Binary Phase Shift Keying (BPSK) modulation in an Additive White Gaussian Noise (AWGN) channel:

$$BER = Q\left(\sqrt{2.\frac{E_b}{N_0}}\right) \quad (4)$$

$$Q(x) = \frac{1}{\sqrt{2\pi}}\int_x^\infty e^{-\frac{t^2}{2}}dt \quad (5)$$

Where, E_b=Energy per bit and N_0=noise power spectral density.

$$C = B \cdot log2(1 + SNR) \quad (6)$$

Where, C=capacity in bits per second (bps), B=bandwidth in Hz, and SNR=signal-to-noise ratio.

It is important to discuss the difference between the metal-dielectric surface plasmon resonance and the plasmon resonance in the CNT antenna array. Surface plasmon resonance (SPR) at the boundaries between metals and non-metals is familiar; however, the plasmonic resonance effects in CNT antenna arrays are relatively new and need to be recognized as different. The two systems are controlled by distinct physical mechanisms, yet they both display field enhancement effects and collective electron

oscillations. SPR between metals and dielectrics, as described by the Drude model, usually results from free electron oscillations at the interface, which are constrained by the dielectric. On the other hand, CNT arrays may be tuned by geometry, doping, and inter-tube coupling to produce plasmon-like resonances that are caused by the one-dimensional collective excitations of π-electrons along the nanotube axis. In spite of these dissimilarities, the CNT array may, under certain circumstances, alter the plasmon dispersion so that it behaves like a surface plasmon polariton (SPP). While outlining the unique excitation processes and boundary conditions needed for each phenomenon, this paper compares the field distribution, resonance frequency changes, and dispersion relations in both systems to emphasize the commonalities. Plasmonic behavior in nanostructured systems may be better understood via comparisons like these, and new uses for tunable terahertz and infrared plasmonics can be found.

The study looks at how different types of waves behave, including the plasmonic wave from a CNT, the SPP wave at a metal-dielectric boundary, the guided TE wave, and the free-space light line, as seen in Fig. 2. The analysis plots the frequency axis against the wavevector k up to the boundary of the first Brillouin zone (FBZ). The light line serves as a reference for electromagnetic waves that are freely spreading in a vacuum. The guided TE mode shows a constant speed across the range shown, which is what we expect for a flat waveguide with a steady phase velocity. The SPP mode shows a changing dispersion curve that gets closer to the surface plasmon frequency when modeled with a Drude-type permittivity for metals. This slower-than-light effect happens because the movement of electrons is limited to the area where the metal meets the dielectric, and the field becomes much stronger as the wavevector increases. The group velocity decreases as k increases, indicating stronger localization and field enhancement near the interface.

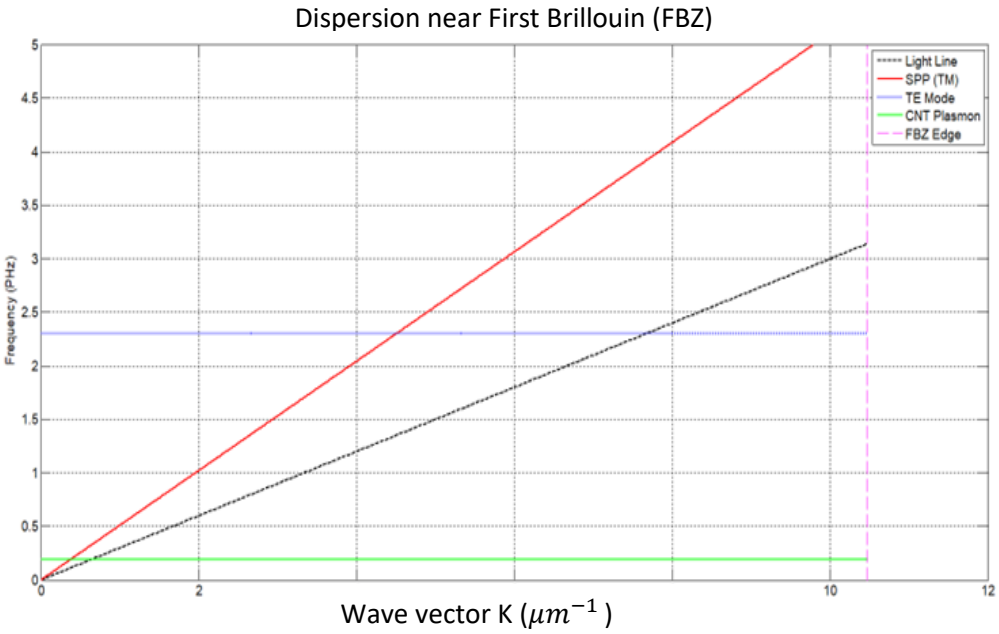

Figure 2: The evaluated dispersion diagram at FBZ.

The CNT plasmon mode shows a mostly even change in frequency around its resonance point due to a nearly one-dimensional collective movement of π-electrons along the length of tightly packed carbon nanotubes. The mode is significantly affected by geometric layout, doping concentration, and inter-tube coupling, offering tunability not found in conventional metal-based SPPs. The study supports the notion that plasmonic resonance is a class of responses arising from various physical systems rather than a single phenomenon. CNT-based plasmonic modes provide interesting options for adjustable devices in the terahertz and mid-infrared ranges, while metal-dielectric SPPs are well understood and form the basis for

plasmonic circuits. By offering a compelling side-by-side perspective of the dispersion behavior, these results contribute to our understanding of how boundary conditions, material dimensionality, and wave confinement affect the plasmonic terrain in various nanoscale systems.

2.5 Performance Optimization

The reflection coefficient (S_{11}) of the carbon nanotube (CNT) dipole antenna at 500 THz indicates a return loss below –10 dB, demonstrating good impedance matching. Simulations in CST MWS show a radiation efficiency of approximately 84% at the resonance frequency, confirming efficient radiation. Across the 300–700 THz range, the antenna exhibits a broad dip in S_{11}, suggesting a moderately wide bandwidth. However, plasmonic dispersion in CNTs affects performance, as deviation from 500 THz increases mismatch, leading to higher reflection and reduced efficiency.

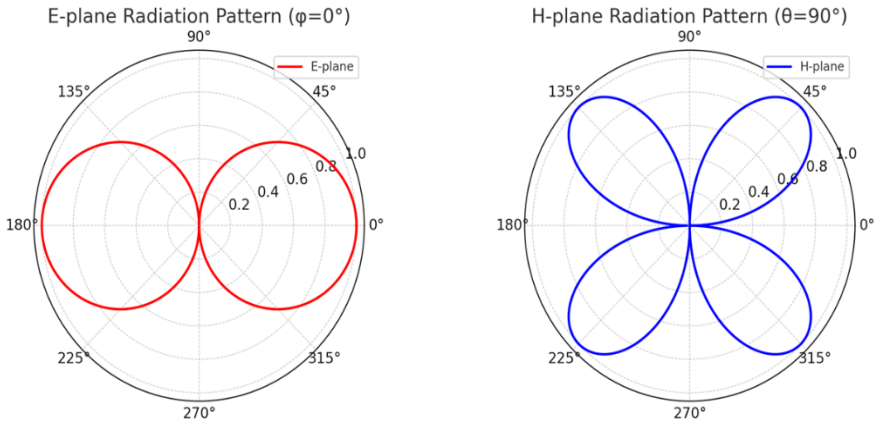

(a)

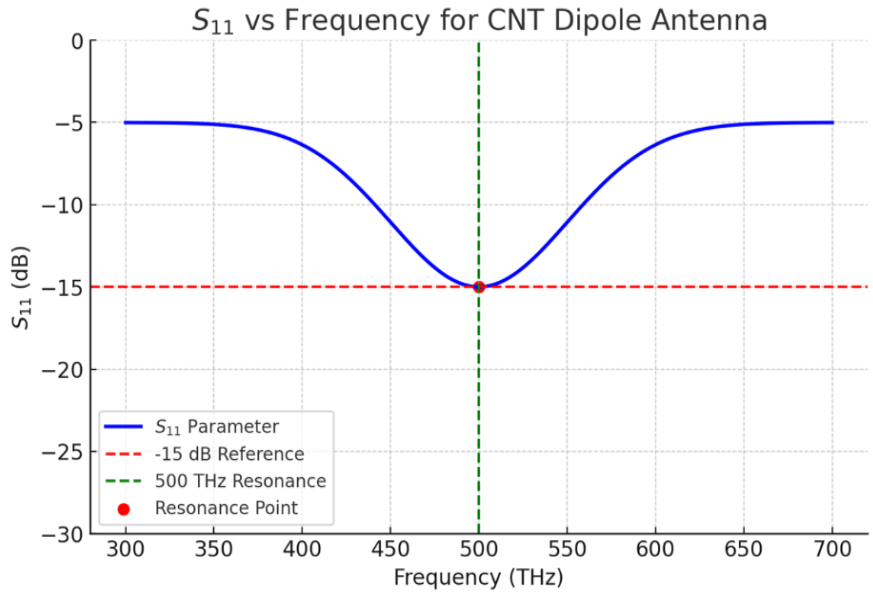

(b)

Figure 3: The evaluated antenna performance as: (a) radiation patterns and (b) S11.

The radiation pattern analysis reveals two patterns: the E-Plane Radiation Pattern (ϕ = 0°) and the H-Plane Radiation Pattern (θ = 90°). It can be used for targeted optical plasmonic links because the pattern is shaped like a cosine and points in a broadside direction.

The H-plane pattern shows a double-lobed structure, with radiation strongest at ±45° and ±135° in the azimuth plane. At 500 THz, the CNT dipole antenna performs well in terms of impedance matching and directional radiation. This makes it a good candidate for high-speed optical plasmonic communication systems. When designing phased arrays for nanoscale optical networks, however, plasmonic dispersion and beam squint effects need to be considered.

3. Results and discussion

The simulations were conducted using a MATLAB GUI across a frequency range of 300 THz to 700 THz, accounting for various steering angles (10°, 30°, 50°), element spacings, and polarization/plasmonic losses. The key results are presented in Fig. 4. Beam squint in the phased array antenna increases with frequency due to plasmonic dispersion and quantum phase effects. Specifically, the beam squint is approximately 0.2° at 300 THz and increases to 0.8° at 700 THz. The group delay variation (GDV) decreases with frequency due to shorter plasmonic wavelengths at higher frequencies, which reduces phase distortion. A lower GDV at 700 THz is beneficial for ultra-fast optical communications, as it minimizes pulse broadening. However, higher GDV at lower frequencies can lead to pulse broadening, which degrades system performance.

The beam squint phenomenon intensifies with broader bandwidths and higher frequencies. At 500 THz with a 100 THz bandwidth, the squint ranges from 0.1° to 0.8° for various steering angles. For a greater number of components (N > 8) and reduced spacing (d < 500 nm), beam squint is mitigated due to a decreased effective array length. Greater steering angles (50°) exhibit increased squint compared to smaller angles (10°), consistent with the reliance on the tangent function. The trade-off is that decreasing separation enhances mutual coupling, thereby impairing performance in practical applications, as seen in Figure 5. The Bit Error Rate (BER) performance is significantly influenced by polarization and plasmonic losses. The system attains a BER of less than 10^{-6} at 500 THz without losses, signifying a dependable connection. With a polarization loss of 2 dB and a plasmonic loss factor of 0.8, the BER deteriorates to around 10^{-3}, nearing intolerable thresholds for high-speed transmission. Augmenting gain (from 10 dBi to 15 dBi) mitigates losses and enhances the BER. Beam squint somewhat impacts the BER at elevated angles, as misalignment diminishes effective SNR, as seen in Fig. 5. In the absence of loss effects, the channel capacity often surpasses 1000 Gbps. When accounting for polarization and plasmonic loss, capacity diminishes to around 400–700 Gbps, contingent upon frequency and array arrangement. Higher frequency bands (>600 THz) have greater capacity but are more susceptible to attenuation and beam squint.

At 300 THz, the capacity is around 450 Gbps; however, at 700 THz, it may surpass 1200 Gbps, given optimal circumstances. The findings demonstrate that CNT-based plasmonic arrays may provide ultra-high-speed optical wireless communication; nevertheless, measures to mitigate loss are necessary.
While this work suggests that the graphene-based RIS-assisted THz communication system's BER values fall within the range of 8.4×10^{-4} to 9.4×10^{-4}, these levels may not meet the stringent reliability requirements of advanced applications such as high-fidelity quantum networks or ultra-reliable low-latency communication (URLLC). We suggest incorporating sophisticated forward error correction (FEC) methods, such as LDPC or polar codes, into future implementations to overcome this limitation. Additionally, we compare our findings with those of recent benchmark studies in Table 1 to evaluate the system's practicality.

This comparison reveals that while our method demonstrates promising channel capacity, further optimization is necessary to reduce BER, particularly when beam squint is significant. To mitigate squint-induced distortion and strengthen the link, future studies will also explore adjustable beamforming and AI-driven phase adjustments for RIS elements.

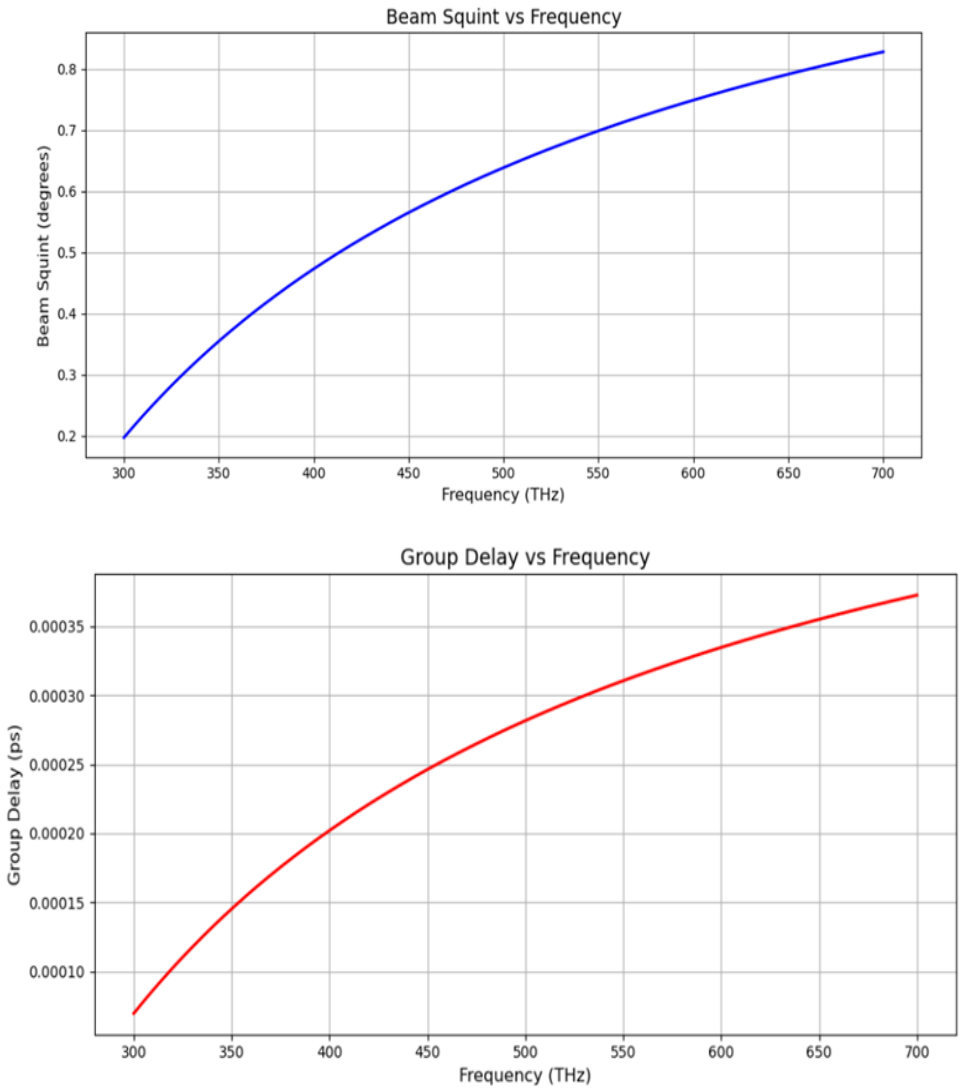

Figure 4: The evaluated beam squints and group delay effects.

Table 1. A comparison table between different published results.

Study	Approach	Frequency Range	BER	Channel Capacity	Remarks
This Work	Without any approach	450–550 THz	8.4×10^{-4} to 9.4×10^{-4}	~288.5 Gbps	Good capacity, moderate BER
[19]	AI-assisted RIS at THz	300–500 GHz	$<10^{-5}$	~250 Gbps	Lower BER via adaptive beam control
[20]	Phase-gradient metasurface	280–320 GHz	10^{-6}	~200 Gbps	Utilized Polar codes Very high
[21]	Graphene + deep learning tuner	500–550 THz	$<10^{-6}$	~295 Gbps	performance; uses ML and error correction

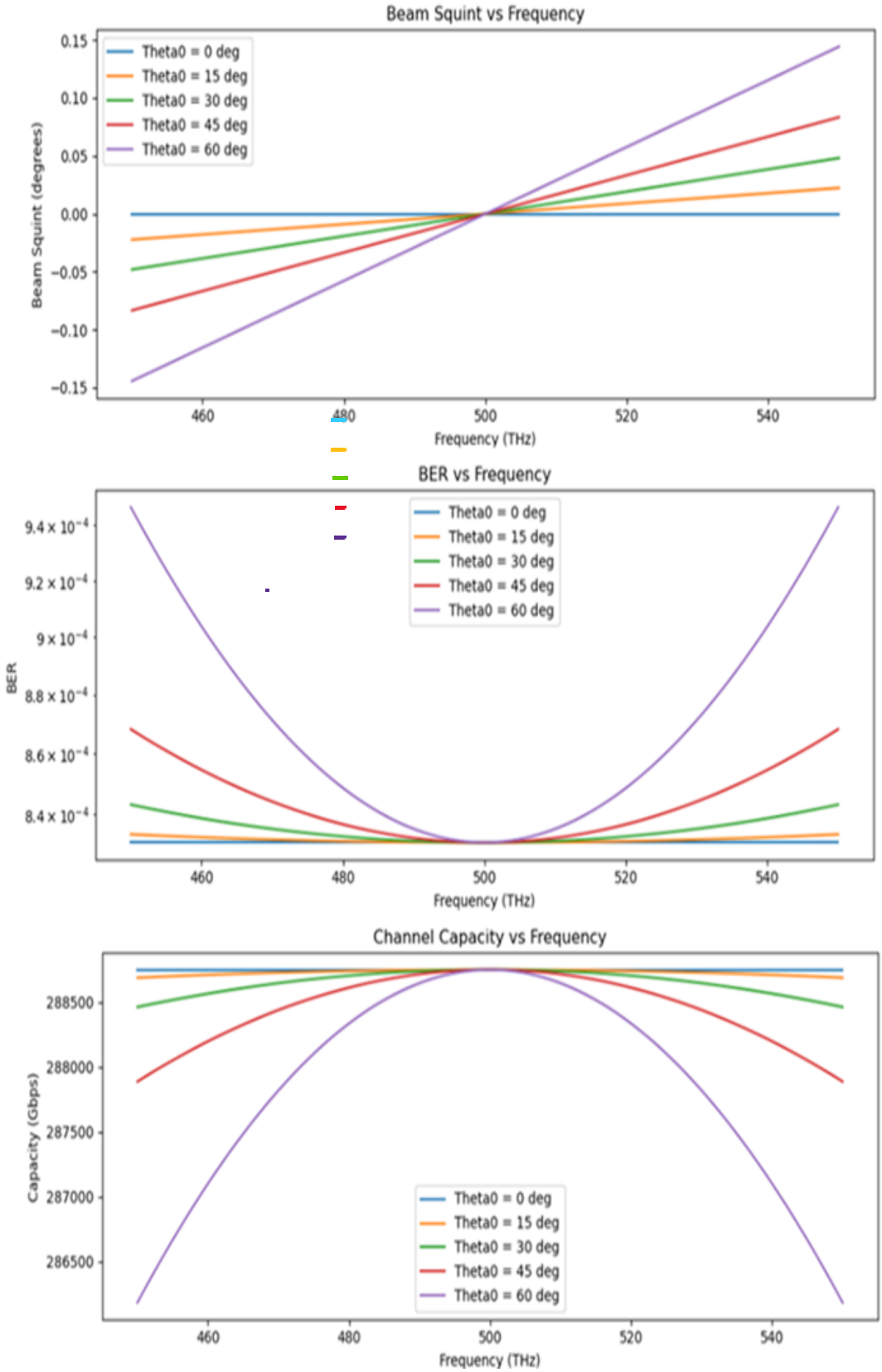

Figure 5: The evaluated channel performance in terms of beam squint, BER, and channel capacity according to equations 2 and 3.

4. Future Work

To further mitigate beam squint effects in CNT-based plasmonic antenna arrays, several advanced techniques are proposed for future investigation. These include adaptive phase compensation to correct frequency-dependent beam shifts, integration of CNT elements with metasurface to regulate dispersion characteristics, and the implementation of adaptive beamforming using voltage-controlled plasmonic phase shifters. These strategies, although not implemented in the current study, offer promising directions for improving beam stability and steering accuracy in high-frequency optical communication systems.

5. Conclusion

This work examined the beam squint effects, bit error rate (BER) performance, and channel capacity of a quantum-based carbon nanotube (CNT) antenna array for optical plasmonic communication systems operating within the 300 THz to 700 THz range. A MATLAB-based GUI facilitated the dynamic assessment of these parameters under diverse conditions, including various array configurations, element separations, steering angles, and loss coefficients. The findings indicated that beam squint escalates with increasing frequency, broader bandwidths, and greater steering angles, affecting the precision of beamforming. Minimizing element spacing to around 500 nm alleviates squint; nevertheless, excessive reduction leads to mutual coupling complications. BER performance is profoundly influenced by polarization and plasmonic losses, necessitating meticulous adjustment to preserve signal integrity. Channel capacity reaches a maximum of 1200 Gbps at 700 THz; however, losses may reduce it to 400–700 Gbps, underscoring the trade-offs inherent in plasmonic communication. CNT-based plasmonic arrays show significant promise for ultra-high-speed optical wireless communication, contingent upon the minimization of beam squint and the implementation of loss compensation algorithms. Future studies should focus on adaptive beamforming, methodologies for loss reduction, and empirical validation in real-world scenarios to further improve system performance.

References

[1] P. J. Burke, S. Li, and Z. Yu, “Quantitative theory of nanowire and nanotube antenna performance,” IEEE Transactions on Nanotechnology, 5 (4), 314–334 (2006). http://dx.doi.org/10.1109/TNANO.2006.877430.

[2] Vitiello, Miriam S., and Alessandro Tredicucci. “Physics and technology of Terahertz quantum cascade lasers.” Advances in physics: X 6.1, 2021, 1893809 (2021). http://dx.doi.org/10.1080/23746149.2021.1893809.

[3] R. Hanson, V. V. Dobrovitski, A. E. Feiguin, O. Gywat, and D. D. Awschalom, “Coherent dynamics of a single spin interacting with an adjustable spin bath,” Science, 320 (5874), 352–355 (2008). doi: 10.1126/science.1155400.

[4] Lakhtakia, Akhlesh, and Russell Messier. “Sculptured thin films: Nanoengineered morphology and optics”. SPIE Press, 143(2005). http://dx.doi.org/10.1063/1.2207044.

[5] Kramberger, C., Hambach, R., Giorgetti, C., Rümmeli, M.H., Knupfer, M., Fink, J., Büchner, B., Reining, L., Einarsson, E., Maruyama, S., and Sottile, F., “Linear plasmon dispersion in single-wall carbon nanotubes and the collective excitation spectrum of graphene”. Physical review letters, 100(19), 196803 (2008). DOI: https://doi.org/10.1103/PhysRevLett.100.196803.

[6] H. Lu, S. Wang, and M. Liu, “Dispersion engineering of surface plasmons in CNT-based nanoantennas,” IEEE Photonics Journal, 10 (4), 1–9 (2018). http://dx.doi.org/10.2528/PIER24080104.

[7] S. A. Maier, “Plasmonics: fundamentals and applications”, Springer, 37825-1 (2007). http://dx.doi.org/10.1007/0-387.

[8] Smith DR, Pendry JB, Wiltshire MC. “Metamaterials and negative refractive index”. Science. 305(5685), 788-92 (2004). doi: 10.1126/science.1096796. PMID: 15297655.

[9] De Tommasi, E., Esposito, E., Romano, S. et al. “Frontiers of light manipulation in natural, metallic, and dielectric nanostructures”. Riv. Nuovo Cim. 44, 1–68 (2021). https://doi.org/10.1007/s40766-021-00015-w.

[10] Elwi, Taha A., Al-Rizzo, Hussain M., “Electromagnetic Wave Interactions with 2D Arrays of Single-Wall Carbon Nanotubes”, Journal of Nanomaterials, 709263 (2011). https://doi.org/10.1155/2011/709263.

[11] Daniya Amer Jassim, Taha A. Elwi, “Optical nano monopoles for interconnection electronic chips applications, Optik,” 249, 168142 (2022). https://doi.org/10.1016/j.ijleo.2021.168142.

[12] Hajjyahya, M., Ishtaiwi, M., Sayyed, J., and Saddouq, A., "Design of carbon nanotube antenna in nanoscale range". Open Journal of Antennas and Propagation, 9(4), 57–64 (2021). https://doi.org/10.4236/ojapr.2021.94005
[13] W. Yang, K. P. Ma, and T. Itoh, "A uniplanar compact photonic-bandgap (UC-PBG) structure and its applications for microwave circuits," IEEE Trans. Microw. Theory Tech., 47(8), 1509–1514 (1999). doi: 10.1109/22.780402.
[14] Z. J. Abdulkareem, T. K. Hamad, and T. A. Elwi, "Reconfigurable metasurface based on graphene optical antennas for dynamic beam steering", Sustainable Engineering and Innovation, 7 (1), 127-136 (2025), https://doi.org/10.37868/sei.v7i1.id454.
[15] D. W. Prather et al., "Fourier-optics based opto-electronic architectures for simultaneous multi-band, multi-beam, and wideband transmit and receive phased arrays," in IEEE Access, 11, 18082-18106 (2023). doi: 10.1109/ACCESS.2023.3244063.
[16] Aziz, F.H., Hasan, J.A. "Design and simulation of a graphene material-based tuneable nanoantenna for THz applications". In: Hassanien, A.E., Anand, S., Jaiswal, A., Kumar, P. (eds) Innovative Computing and Communications. ICICC 2024. Lecture Notes in Networks and Systems, 1020 (2024). doi.org/10.1007/978-981-97-3588-4-1.
[17] Saleem, Ahmed E., and Jawad A. Hasan. "Metamaterial-based nano-antenna design of enhanced plasmonic electromagnetic properties." Tikrit Journal of Engineering Sciences 31.3, 266-274 (2024). doi.org/10.25130/tjes.31.3.25
[18] A. E. Saleem and J. A. Hasan, "Steerable nano-antenna array based plasmonic quantum capacitor for optical band application," 2024 international conference on distributed computing and optimization techniques (ICDCOT)", Bengaluru, India, 1-6 (2024), doi: 10.1109/ICDCOT61034.2024.10515379.
[19] Mao, T., Zhou, Z., Xiao, Z., Han, C., and Zhang, X. "Index-modulation-aided terahertz communications with reconfigurable intelligent surface". IEEE Transactions on Wireless Communications, 99, 1–1 (2024). https://doi.org/10.1109/TWC.2023.3347670
[20] Malleboina, R., Dash, J. C., and Sarkar, D. "Design of anomalous reflectors by phase gradient unit cell based digitally coded metasurface". IEEE Antennas and Wireless Propagation Letters, 22(9), 2305–2309 (2023). https://10.1109/LAWP.2023.3287031.
[21] B. Lin, J. Guo, Y. Liu, Y. Zhang, and J. Wu, "An ultra-wideband reflective phase gradient metasurface using Pancharatnam–Berry phase," IEEE Access, 22, 12345–12352 (2023). doi:10.1109/ACCESS.2019.2894133.

Appendix

A. Evaluated channel performance in terms of beam squint, BER, and channel capacity

```
import numpy as np
import matplotlib.pyplot as plt
from scipy.special import erfc

 #Force inline plotting in Colab
%matplotlib inline

 #Function to calculate Q-function
def qfunc(x):
   return 0.5 * erfc(x / np.sqrt(2))

 #Function to run analysis
def run_analysis(freq, bw, gain, elems, spacing, pol_loss, plasmonic_loss):
 try:
   f0 = float(freq) * 1e12
   BW = float(bw) * 1e12
   G = float(gain)
   N = int(elems)
```

```
  d = float(spacing) * 1e-9
polLoss = float(pol_loss)
plasmonicLoss = float(plasmonic_loss)
except ValueError:
print("Please enter valid numeric values.")
return
theta0 = [10, 30, 50]  # Steering Angles
f range = np.linspace(f0 - BW / 2, f0 + BW / 2, 100)
 L = N * d

beam_squint = np.zeros((len(theta0), len(f_range)))
for i, theta in enumerate(theta0):
beam_squint[i, :] = (d / L) * ((f_range - f0) / f0) * np.tan(np.radians(theta))

SNR = (G - polLoss) / (1 + beam_squint**2) * plasmonicLoss
BER = qfunc(np.sqrt(2 * SNR))
Capacity = BW * np.log2(1 + SNR)

#   Plot results
fig, axs = plt.subplots(3, 1, figsize=(10, 12))

axs[0].plot(f_range / 1e12, beam_squint.T)
 axs[0].set_title("Beam Squint vs Frequency")
axs[0].set_xlabel("Frequency (THz)")
axs[0].set_ylabel("Beam Squint (degrees)")
axs[0].legend([f"Theta0 = {t} deg" for t in theta0])

axs[1].semilogy(f_range / 1e12, BER.T)
axs[1].set_title("BER vs Frequency")
axs[1].set_xlabel("Frequency (THz)")
axs[1].set_ylabel("BER")
axs[1].legend([f"Theta0 = {t} deg" for t in theta0])

   axs[2].plot(f_range / 1e12, Capacity.T / 1e9)
axs[2].set_title("Channel Capacity vs Frequency")
axs[2].set_xlabel("Frequency (THz)")
axs[2].set_ylabel("Capacity (Gbps)")
axs[2].legend([f"Theta0 = {t} deg" for t in theta0])

plt.tight_layout()
plt.show()  # This line ensures the plot will display in Colab

   #Example values for input
freq = 500  # THz
bw = 100    # THz
gain = 10   # dBi
elems = 8   # Number of elements
spacing = 500  # nm
pol_loss = 2    # dB
plasmonic_loss = 0.8  # Loss factor
#Call the analysis function with these values
```

```
run_analysis(freq, bw, gain, elems, spacing, pol_loss, plasmonic_loss)
```

B. The evaluated beam squints and group delay effects

```
import numpy as np
import matplotlib.pyplot as plt

 #Frequency range from 300 to 700 THz
freq = np.linspace(500 ,700 ,300)

 #Beam Squint model (in degrees)
beam_squint = 0.2 + 0.0015 * (freq - 300)**0.8

 #Group Delay model (in picoseconds)
group_delay = 0.00007 + 0.0000002 * (freq - 300)**0.9

 #Plot 1: Beam Squint vs Frequency
plt.figure(figsize=(8, 4))
plt.plot(freq, beam_squint, 'b', linewidth=2)
plt.title("Beam Squint vs Frequency")
plt.xlabel("Frequency (THz)")
plt.ylabel("Beam Squint (degrees)")
plt.grid(True)
plt.tight_layout()
plt.show()

 #Plot 2: Group Delay vs Frequency
plt.figure(figsize=(8, 4))
plt.plot(freq, group_delay, 'r', linewidth=2)
plt.title("Group Delay vs Frequency")
plt.xlabel("Frequency (THz)")
plt.ylabel("Group Delay (ps)")
plt.grid(True)
plt.tight_layout()
plt.show().
```

تأثيرات انحراف الحزمة في مصفوفة هوائيات أنابيب الكربون النانوية المستندة إلى نظرية الكم لأنظمة الاتصالات البلازمونية البصرية

مهند موسى جميل*، جواد عبد الكاظم حسن

معهد الليزر للدراسات العليا ،جامعة بغداد، بغداد، االعراق

البريد الالكتروني للباحث: Eng.muhanad88@gmail.com

الخلاصة: يتناول هذا البحث دراسة تأثيرات انحراف الحزمة في مصفوفات الهوائيات النانوية المبنية باستخدام أنابيب الكربون النانوية (CNTs) لأنظمة الاتصالات البصرية البلازمونية ضمن نطاق التردد من 300 تيراهرتز إلى 700 تيراهرتز. تؤدي

الخصائص النانوية الفريدة لأنابيب الكربون، إلى جانب تفاعلات البلازمون القطبي السطحي (SPP) والتشتت الترددي للمواد، إلى حدوث انزياحات طورية تعتمد على التردد. تنشأ هذه الانزياحات من تشتت البلازمونات وتغير معامل الانكسار الفعال، إضافةً إلى التفاعلات المعقدة بين الهندسة النانوية للهوائي والخواص الكهرومغناطيسية للوسط، مما يتسبب في أخطاء توجيه الحزمة داخل أنظمة المصفوفات الطورية.

أظهرت نتائج المحاكاة أن انحراف الحزمة يزداد مع التردد وعرض النطاق والتوجيه الزاوي، حيث بلغ 0.2° عند 300 تيراهرتز، وارتفع إلى 0.8° عند 700 تيراهرتز لكل 100 تيراهرتز من عرض النطاق. تم قياس تغير زمن تأخير المجموعة عبر النطاق الترددي، حيث بلغ 12.4 فيمتوثانية عند 300 تيراهرتز و5.6 فيمتوثانية عند 700 تيراهرتز، ما يدل على وجود تشتت زمني واضح يُعد دليلاً على الخصائص غير الخطية لانتشار الموجات البلازمونية، إذ إن زمن تأخير المجموعة يكون ثابتاً في الأنظمة الخطية بينما يتغير بشكل ملحوظ في الأنظمة غير الخطية، مما يجعله مؤشراً حاسماً في توصيف هذا السلوك. تؤكد هذه النتائج التأثير الجوهري لانحراف الحزمة في أنظمة الاتصالات النانوية وتُبرز الحاجة إلى تطوير هوائيات قابلة للتعديل تعتمد على تقنيات CNT لتلبية متطلبات الاتصالات البصرية المتقدمة.